Sensitive dependence of the motion of a legged robot on granular media

Chen Li [*], **Paul B. Umbanhowar** [†], **Haldun Komsuoglu** [‡], **Daniel E. Koditschek** [‡], **Daniel I. Goldman** [*]

[*]School of Physics, Georgia Institute of Technology, Atlanta, GA 30332, [‡]Department of Electrical and Systems Engineering, University of Pennsylvania, Philadelphia, PA 19104, and [†]Department of Mechanical Engineering, Northwestern University, Evanston, Illinois 60208

Submitted to Proceedings of the National Academy of Sciences of the United States of America

Legged locomotion on flowing ground (*e.g.* granular media) is unlike locomotion on hard ground because feet experience both solid- and fluid-like forces during surface penetration. Recent bio-inspired legged robots display speed relative to body size on hard ground comparable to high performing organisms like cockroaches but suffer significant performance loss on materials like sand. In laboratory experiments we study the performance (speed) of a small (2 kg) six-legged robot, SandBot, as it runs on a bed of granular media (1 mm poppy seeds). For an alternating tripod gait on the granular bed, standard gait control parameters achieve speeds at best two orders of magnitude smaller than the 2 bodylength/s (≈ 60 cm/s) for motion on hard ground. Empirical adjustment of these control parameters away from the best hard ground settings can restore the 30 cm/s performance. Robot speed depends sensitively on the packing fraction ϕ and the limb frequency ω, and a dramatic transition from walking to slow swimming locomotor modes occurs when ϕ becomes small enough and/or ω large enough. For hard surfaces, the forces developed during leg-ground contact that accelerate the robot are poorly understood. The corresponding forces on flowing ground remain unexplored. We propose a kinematic model of the walking mode based on generic features of penetration and slip of a curved limb in granular media. The model captures the dependence of robot speed on limb frequency and the transition between walking and swimming modes but highlights the need for a deeper understanding of the physics of granular media.

granular media | robotics | locomotion | control

Compared to agile terrestrial organisms, most man-made vehicles possess limited mobility on complex terrain [1] and are easily thwarted by materials like rubble and sand. Increased locomotive performance of engineered platforms demands better understanding of interaction with complex environments. At the same time, there is increasing evidence that small legged machines can have greater maneuverability than large wheeled vehicles in many natural environments [2]. However, while wheeled and treaded locomotion on sand has been well studied by pioneers like Bekker [3], study of the interaction of animals or legged devices with complex media like sand is in its infancy [4], in part because the physics of penetration and drag in granular media is largely unexplored for realistic conditions. Nearly all previous experiments and models of terrestrial locomotion were developed for running and walking on rigid, flat, non-slip substrates in which the possibility of substrate flow has been ignored [5] [6] [7] [8] [9].

Rainforest, grassland, polar tundra, mountains, and desert are examples of complex Earth terrains where locomotion can be challenging, and the limited experience of the Mars Rovers supports the presumption that extraterrestrial landscapes will be even more daunting. Deserts, common in nature and occupying about 10 percent of land surface on Earth [10], consist largely of granular media, a representative complex substrate. Granular materials, generically defined as collections of discrete particles, can exhibit solid-like [11] behavior below a critical yield stress [12], while liquid-like [13], gas-like [14], and even glass-like [15] behaviors are possible during flow. Yet, compared to other complex materials like debris, mud or snow, granular materials are simple enough that fundamental understanding of the collective physics can be achieved through interplay of experiment and theory. Unlike more heterogeneous real-world environments, granular media can be precisely controlled using laboratory scale devices [15, 16] to create states of varying material strength that mimic different deformable flowing materials produced during locomotion on complex terrains. Here we systematically explore the performance of a small legged device on granular media prepared in different packing states with volume fraction ranges typical of desert sand [17]. We find that locomotion is remarkably sensitive to substrate preparation and gait characteristics, which points to both the need for a more sophisticated understanding of the physics of motion within granular media and the possibility of better robotic control paradigms for locomotion on complex terrains.

Results and Discussion

The robot we study, SandBot (Fig. 1a), is the smallest in a successful series of six legged robots, the RHex class [18]. SandBot moves using an alternating tripod gait, such that two sets of three approximately c-shaped limbs rotate synchronously and π out of phase. By controlling a clock signal (Fig. 1c), we prescribe the angular trajectory of each tripod. On rigid, no-slip ground SandBot's limb trajectories are tuned to create a bouncing locomotion [18] that generates speeds up to 2 body-lengths/sec. We initially used this clock signal on granular media, but found that the robot instead of bouncing adopts a swimming gait in which the legs always slip backward relative to the stationary bed and for which performance is reduced by a factor of 30 (see Supporting Information Movie S1). We surmised that this was due to an interval of double stance (both tripods in simultaneous contact with the ground), which is useful on hard ground during bouncing gaits but apparently causes tripod interference on granular media. Changes to the clock signal removed the double stance and slowed the initial leg impact. These parameter modifications allowed SandBot to move (see Movie S2) in the granular media at speeds up to 30 cm/s (1 body-length/sec) in a walking gait that resembled the pendular gait of the robot on hard ground [19] but with important kinematic differences (to be discussed below). No amount of limb parameter adjustment produced rapid bouncing locomotion.

Reserved for Publication Footnotes

In the desert, robots can encounter granular media ranging in volume fraction from $\phi = 0.55$ to $\phi = 0.64$ [17]. To test the robot performance on controlled volume fraction granular media, we employ a 2.5 m long fluidized bed trackway (Fig. 1b) [20], which allows the flow of air through a bed of granular media, in this case $\sim$ 1 mm poppy seeds. With initial fluidization followed by repeated pulses of air [21], we prepare controlled volume fraction states with different penetration properties [22]. In this study, we test the performance of SandBot with varied limb frequency for ϕ states ranging from loosely to closely packed ($\phi = 0.580$ to $\phi = 0.633$). We hypothesized that limb frequency would be important to robot locomotion since the substrate yield strength increases with increasing ϕ and the yield stress divided by the robot limb area $\times$ mass $\times$ velocity is proportional to the maximum limb frequency for efficient locomotion.

We find that robot performance is remarkably sensitive to ϕ (see Movie S3). For example, at $\omega = 16$ rad/s the robot speed $v(t)$ shows a change in average velocity $\overline{v}_x$ of nearly a factor of five as ϕ changes by just 5 % (Figs. 1d,e). For the closely packed state ($\phi = 0.633$), $\overline{v}_x$ was approximately 20 cm/s with $\sim$ 5 cm/s oscillations during each tripod rotation, whereas for a more loosely packed state ($\phi = 0.600$), $\overline{v}_x \approx 2$ cm/s with 1 cm/s variations in velocity.

This sensitivity to volume fraction is shown in the average robot speed vs. volume fraction (Fig. 1e). For fixed ω, $\overline{v}_x$ is effectively constant for ϕ above a critical volume fraction $\phi_c(\omega)$, but is close to zero for ϕ below $\phi_c(\omega)$. For fixed ω, $\phi_c(\omega)$ separates volume fraction into two regimes: the "walking" regime ($\phi \geq \phi_c$, $\overline{v}_x >> 0$) and the "swimming" regime ($\phi < \phi_c(\omega)$, $\overline{v}_x \approx 2$ cm/sec). See Movie S4 and Movie S5 for examples of walking and swimming modes.

Walking is dominant at low ω and high ϕ. In this mode, the leg of a tripod penetrates down and backward into the ground until the granular yield stress exceeds the limb transmitted inertial and gravitational stresses at a depth $d(\omega, \phi)$. At this point, rather than rolling forward like a wheel, each semi-circular limb abruptly stops translating relative to the grain bed and starts rotating about its now stationary center of curvature by slipping tangentially relative to the grains in the circular depression surrounding the limb (see Fig. 3a). This rotary motion propels the axle and consequently the rest of the robot body along a circular trajectory in the $x - z$ plane with speed $R\omega$, where $R = 4$ cm is the radius of the c-leg. The forward body motion ends when, depending on ϕ and ω, either the second tripod begins to lift the robot or the underside of the robot again contacts the ground. With increased ω limbs penetrate further as the inertial force of rapidly accelerating the robot body to the finite limb velocity increases. As the penetration depth approaches its maximum $2R - h$, where h is the height of the axle above the flat undercarriage of the robot, the walking step size goes to zero. Any subsequent forward motion is due solely to thrust forces generated by the swimming-like relative translational motion of the limb though the ground. Note that $\phi_c(\omega)$ increases with ω, and that the transition of $\overline{v}_x$ from walking to swimming is sharper for higher ω and smoother for lower ω. The much slower swimming mode occurs for all volume fractions for $\omega \geq 30$ rad/s.

Plotting the average robot speed as a function of limb frequency (Fig. 2a) shows how the robot suffers performance loss as its legs rotate more rapidly. For fixed ϕ, $\overline{v}_x$ increases sub-linearly with ω to a maximal speed $\overline{v}_x^*$ at a critical limb frequency ω_c, above which $\overline{v}_x$ quickly decreases to near zero (swimming) [23]. The robot suffers partial performance loss (mixed walking and swimming) below ω_c and near total performance loss (pure swimming) above ω_c. Performance loss for $\phi \gtrapprox 0.6$ is more sudden (total performance loss within 1 rad/s) compared to performance loss for $\phi \lessapprox 0.6$. Both ω_c and $\overline{v}_x^*$ display transitions at $\phi \approx 0.6$ (Figs. 2b,c). The transition at $\phi \approx 0.6$ for the rapidly running robot is noteworthy since it has been observed that granular media undergo a transition in quasi-static penetration properties for $\phi \approx 0.6$ [22].

We developed a two-parameter model that agrees well with the data (dashed lines in Fig. 2a) and is based on the dominant mode, walking with circular slipping. The model incorporates the observed limb kinematics and a simplified force law for granular penetration and indicates that reduction of step length through increased penetration depth is the cause of the sub-linear increase in $\overline{v}_x$ with ω. The model assumes that the two tripods act independently of each other and that the motion of each tripod can be understood by examining the motion of a single c-leg supporting a mass m equal to one-third of Sandbot's total mass. The most important component of the model is the limb penetration depth, which is determined by balancing the granular penetration force [24], kz, with the sum of the gravitational and inertial forces $m(a + g)$, where $k(\phi)$ characterizes the ground penetration resistance, d is the depth below the bed surface of the lowest point on the limb, a is the acceleration magnitude of the robot center of mass, and g is the acceleration due to gravity. Taking the acceleration of the robot when the limb comes to rest as $a = R\omega/\Delta t$ where Δt is the characteristic elastic response time of the leg and grain bed, gives the maximum leg penetration depth $d_{max} = \frac{m}{k}(\frac{R\omega}{\Delta t} + g)$. Assuming that the the undercarriage rests on the surface at the beginning of the ground contact phase and using the geometry of rotary walking (see Fig. 3a), the walking step size per leg rotation is $s = 2\sqrt{R^2 - (d_{max} + h - R)^2}$. Since there are two leg rotations per period (one from each tripod), $\overline{v}_x = \frac{\omega s}{\pi} = \frac{2\omega}{\pi}\sqrt{R^2 - \left[\frac{m}{k}(\frac{R\omega}{\Delta t} + g) + h - R\right]^2}$.

The fit parameter k increases monotonically with ϕ from 1.7e5 to 2.2e5 N/m and varies rapidly below $\phi \approx 0.6$ and less rapidly above. Its average value of 2.0e5 N/m corresponds to a shear stress per unit depth of approximately 4000 N/m^3 which is consistent with previous measurements of ground penetration properties [25]. In contrast, Δt varies little with ϕ and has an average value of 0.4 sec which compares favorably with the robot's measured hard ground oscillation period when supported on a single tripod of 0.2 sec. In the model we assume the two tripods do not simultaneously contact the ground, however, in soft ground this is not the case which consequently reduces the effective step size per period from $2s$ to a lesser value. The fit value of Δt is sensitive to this variation; reducing the step size per period by just 13 % decreases Δt to 0.2 sec while k is increased by less than 10 %.

Our model indicates that for deep penetration the walking step length is quite sensitive to penetration depth. As the walking step size goes to zero with increasing ω or decreasing ϕ, the fraction of the ground contact time that the leg slips through the grains (swimming) goes to one. Swimming in granular media differs from swimming in simple fluids as the friction dominated thrust and drag forces are largely rate independent at slower speeds [26, 24]. When thrust exceeds drag, the robot advances a distance proportional to the net force divided by ω^2 per leg rotation, and, consequently, velocity is proportional to ω^{-1}. This explains the weak dependence of $\overline{v}_x$ on ω in the swimming mode. (The increase in robot velocity with decreasing ω is bounded by the condition that the robot center of mass velocity in the ground (lab) reference frame cannot exceed the horizontal leg speed in the center of

mass coordinates of the robot, which ensures the existence of and eventual transition to a walking mode as ω is decreased.)

The transition from walking to swimming appears gradual for $\phi \lessapprox 0.6$ since the penetration depth increases slowly with ω and the ω^{-2} contribution to the per step displacement from swimming is relatively large (see *e.g.* the data at $\omega = 12$ rad/sec in Fig. 3b). However, for $\phi \gtrapprox 0.6$, the transition is abrupt. We hypothesize that this sharp transition occurs because the per step displacement is reduced sufficiently that the legs encounter ground disturbed by the previous step. At higher ϕ, the volume fraction of the disturbed ground is significantly less compared to the bulk which increases penetration and consequently reduces the walking step size to near zero; this is not the case for the transition from walking to swimming at low ϕ (and low ω) where the ϕ of the disturbed material is relatively unchanged relative to its initial value. The disturbed ground hypothesis is supported by calculations of the step length using the average velocity $s = 2\pi\overline{v}_x/\omega$ which clearly show a critical step length $s_c = 7$ cm (nearly equal to the 7.1 cm limb diameter) at the walking/swimming transition (Fig. 3d). Signatures of failure (see online supplemental material) are also evident in lateral views of the robot kinematics and measurements of the robot body tilt angle (β in Fig. 1b).

At higher ω in the swimming mode, the limbs move with sufficient velocity to fling material out of their path and form a depression which reduces thrust because the limbs are not as deeply immersed on subsequent passes through the material. However, as limb velocity increases, thrust forces becomes rate dependent and increase because the inertia imparted to the displaced grains is proportional to ω^2. Between strokes, the excavated depression re-fills at a rate dependent on the difference between the local surface angle and the angle of repose [27] and the depression size. Investigating the competition between these different processes at high ω and their consequences for locomotion could be relevant to understanding how to avoid becoming stranded or to free a stranded device.

Conclusions

Our studies are the first to systematically investigate the performance of a legged robot on granular media (e.g. volume fraction and rate dependence) and show how precarious it can be to move on such complex material; changes in ϕ of less than one percent result in either rapid motion or failure to move. Slight kinematic changes have similar effect. We propose that a detailed understanding of the effects of thrust and drag on locomotion will require advances in understanding of volume fraction effects on transient events like impact, penetration, crater collapse, and surface drag. Further studies of this kind can lead to theory of interaction with complex media advanced enough to predict limb design and control, similar to the well-developed models of aerial and aquatic craft. For example, adaptation of kinematic variables such as step length [28] to varying substrate properties could result in substrate optimized control strategies. Analysis of physical models such as SandBot can also inform locomotion biology in understanding how animals appear to move effortlessly across a diversity of complex substrates [29, 30]. Such devices will begin to have capabilities comparable to organisms; these capabilities could be used for more efficient and capable exploration of challenging terrestrial (*e.g.* rubble and disasters sites) and extra-terrestrial (*e.g.* the Moon and Mars) environments.

Materials and Methods

Limb kinematics SandBot is a hexapedal robot platform that borrows its morphological design from the successful RHex class [18] [31]. SandBot's motors are controlled to follow the same prescribed kinematic path during each rotation and, as shown in previous work on RHex, changes in this kinematics have substantial effects on robot locomotor performance [32]. The kinematic angular trajectory consists of a fast phase and a slow phase with respective angular frequencies. Essentially, the fast phase corresponds to the swing phase (aerial phase), while the slow phase corresponds to the stance phase (ground phase). A set of three parameters uniquely determines the clock signal configuration: θ_s, the angular span of the slow phase; θ_0, the angular position of the center of the slow phase; and d_c, the duty cycle of the slow phase. Specifying the cycle averaged limb angular frequency ω fully determines the motion.

In our initial experiments we tested two sets of clock signals: a hard ground clock signal (HGCS) with ($\theta_s = 0.85$ rad, $\theta_0 = 0.13$ rad, $d_c = 0.56$) which generates a fast bouncing gait (1 m/s) on hard ground [18] but very slow ($\sim$ 1 cm/s) motion on granular media, and a soft ground clock signal (SGCS) with ($\theta_s = 1.1$ rad, $\theta_0 = -0.5$ rad, $d_c = 0.45$) which produces unstable motion on hard ground but regular motion on granular media. This confirmed that the locomotor capacity of SandBot is sensitive to the clock signal. Careful observation of limb kinematics revealed that the hard ground clock signal fails on granular media because of the simultaneous stance phase of two tripods. Also, the SGCS has a slower and delayed slow phase, which suggests that the speed and timing of limb placement may be critical to locomotion on granular media. In this study, we keep the clock signal fixed (SGCS), and explore robot performance as a function of limb frequency and substrate volume fraction.

Integrated sensors record the position and current (and thus torque) of Sandbot's motors vs. the internal time. Comparison of the motor trajectory in experiment with the prescribed motion for both sets of timing parameters confirm a high degree of fidelity with an error of a few percent. Therefore, SandBot's change in performance between HGCS and SGCS timing comes from the physics of the substrate interaction.

Trackway volume fraction control To systematically test SandBot's performance vs. substrate volume fraction, we employ a 2.5 m long, 0.5 m wide fluidized bed trackway with a porous plastic (Porex) flow distributor (thickness 0.64 cm, average pore size 90 μm). Four 300 LPM leaf blowers (Toro) provide the requisite air flow. Poppy seeds were chosen as the granular media because they are similar in size to natural sand [33]. and are of low enough density to be fluidized. The air flow across the fluidized bed is measured with an anemometer (Omega Engineering FMA-900-V) and is uniform to within 10 percent.

A computer controlled fluidization protocol sets the volume fraction and thus the mechanical properties of the bed. A continuous air flow initially fluidizes the granular media in the bubbling regime. The flow is slowly turned off leaving the granular media in a loosely packed state ($\phi = 0.580$). Short air pulses (ON/OFF time = 100/1000 msec) pack the bed [21]. Increasing the number of pulses increases ϕ up to a maximum of $\phi = 0.633$. Volume fraction was calculated by $\phi = m/\rho V$. The mass was measured with a precision scale (Setra). The density of the granular media was measured by means of displacement in water. In experiment, since the area of the fluidized bed trackway is fixed, volume fraction is set by controlling the height of the granular media, $\phi = m/\rho A h$.

Kinematics measurements To characterize SandBot's motion, we record simultaneous dorsal and lateral views with synchronized high speed video cameras (AOS Switzerland) at 100 frames/s. The center of mass (dorsal landmark) and the axles of the right-side front and rear motors (lateral landmarks) are marked with reflective material (WhiteOut). A pulley/rail system allows the power and communication cables to follow the robot as it moves. For each trial, we prepare the trackway with the desired volume fraction and place the robot on the prepared granular media at the far end of the trackway with both tripods in the same standing position. An LED on the robot synchronizes the video and robot motor sensor data. After each trial, Matlab (The MathWorks) is used to obtain landmark coordinates from the video frames and calculate the kinematic variables v and β. Three trials were run for each state of (ϕ, ω).

ACKNOWLEDGMENTS. ACKNOWLEDGEMENTS. We thank Daniel Cohen, Andrew Slatton and Adam Kamor for helpful discussion. This work was supported by the Burroughs Wellcome Fund (D.I.G, C.L, P.B.U).

1. Kumagai, J (2004) Sand trip - Darpa's 320-kilometer robotic race across the mojave desert yields no winner, but plenty of new ideas. Ieee Spectrum 41:44–50.
2. Raibert, MH (1986) Legged robots. Communications of the Acm 29:499–514.
3. Bekker, M (1956) Theory of Land Locomotion (The University of Michigan Press).
4. Kadanoff, LP (1999) Built upon sand: Theoretical ideas inspired by granular flows. Reviews of Modern Physics 71:435–444.
5. Altendorfer, R, Koditschek, DE, Holmes, P (2004) Stability analysis of legged locomotion models by symmetry-factored return maps. International Journal of Robotics Research 23:979–999.
6. Schaal, S, Atkeson, CG, Sternad, D (1996) One-handed juggling: A dynamical approach to a rhythmic movement task. Journal of Motor Behavior 28:165–183.
7. Burridge, RR, Rizzi, AA, Koditschek, DE (1999) Sequential composition of dynamically dexterous robot behaviors. International Journal of Robotics Research 18:534–555.
8. Berkemeier, MD, Fearing, RS (1998) Sliding and hopping gaits for the underactuated acrobot. Ieee Transactions on Robotics and Automation 14:629–634.
9. Westervelt, ER, Buche, G, Grizzle, JW (2004) Experimental validation of a framework for the design of controllers that induce stable walking in planar bipeds. International Journal of Robotics Research 23:559–582.
10. Ezcurra, E (2006) Global Deserts Outlook (United Nations Educational), p 168.
11. Terzaghi, K (1943) Theoretical soil mechanics (New York: Wiley), p 510.
12. Nedderman, R (1992) Statics and kinematics of granular materials (Cambridge University Press), p 352.
13. Heil, P, Rericha, EC, Goldman, DI, Swinney, HL (2004) Mach cone in a shallow granular fluid. Physical Review E 70:060301–060304.
14. van Zon, JS et al. (2004) Crucial role of sidewalls in velocity distributions in quasi-two-dimensional granular gases. Physical Review E 70:040301–040304.
15. Goldman, DI, Swinney, HL (2006) Signatures of glass formation in a fluidized bed of hard spheres. Physical Review Letters 96:174302–174305.
16. Goldman, DI, Korff, WL, Wehner, M, Berns, MS, Full, RJ (2006) The mechanism of rapid running in weak sand. Integrative and Comparative Biology 46:E50–E50 Goldman, D. I. Korff, W. L. Wehner, M. Berns, M. S. Full, R. J.
17. (2008) personal communication from Professor Michel Louge based on field observations in the Sahara desert.
18. Saranli, U, Buehler, M, Koditschek, DE (2001) Rhex: A simple and highly mobile hexapod robot. International Journal of Robotics Research 20:616–631.
19. Altendorfer, R et al. (2001) Rhex: A biologically inspired hexapod runner. Autonomous Robots 11:207–213.
20. Jackson, R (2000) The Dynamics of Fluidized Particles (Cambridge University Press), p 339.
21. Schroter, M, Goldman, DI, Swinney, HL (2005) Stationary state volume fluctuations in a granular medium. Physical Review E 71:030301–030304.
22. Schroter, M, Nagle, S, Radin, C, Swinney, HL (2007) Phase transition in a static granular system. Europhysics Letters 78:44004–44007.
23. We varied ω with 1 rad/s resolution near the transition to locate the exact critical volume fraction ω_c.
24. Albert, R, Pfeifer, MA, Barabasi, AL, Schiffer, P (1999) Slow drag in a granular medium. Physical Review Letters 82:205–208.
25. Stone, MB et al. (2004) Local jamming via penetration of a granular medium. Physical Review E 70:041301–041310.
26. Wieghardt, K (1975) Experiments in granular flow. Annual Review of Fluid Mechanics 7:89–114.
27. de Vet, S, de Bruyn, J (2007) Shape of impact craters in granular media. Physical Review E 76:041306–041311.
28. Hodgins, JK, Raibert, MH (1991) Adjusting step length for rough terrain locomotion. Ieee Transactions on Robotics and Automation 7:289–298.
29. Goldman, DI, Chen, TS, Dudek, DM, Full, RJ (2006) Dynamics of rapid vertical climbing in cockroaches reveals a template. Journal of Experimental Biology 209:2990–3000.
30. Spagna, JC, Goldman, DI, Lin, PC, Koditschek, DE, Full, RJ (2007) Distributed mechanical feedback in arthropods and robots simplifies control of rapid running on challenging terrain. Bioinspiration and Biomimetics 2:9–18.
31. Koditschek, DE, Full, RJ, Buehler, M (2004) Mechanical aspects of legged locomotion control. Arthropod Structure and Development 33:251–272.
32. Seipel, J, Holmes, P (2007) A simple model for clock-actuated legged locomotion. Regular and Chaotic Dynamics 12:502–520 Seipel, J. Holmes, P.
33. Bagnold, RA (1954) The Physics of Blown Sand and Desert Dunes (Methuen and Co. Ltd.), p 265.

Fig. 1. Locomotion of a legged robot on granular media is sensitive to substrate packing and limb frequency. (a) The six-legged robot, SandBot, moves with an alternating tripod gait (alternate triplets of limbs rotate π out of phase); arrows indicate members of one tripod. (b) Pulses of air through the bottom of the fluidized bed trackway control the initial volume fraction ϕ of the granular substrate; air is turned off before the robot begins to move. (c) Tripod leg-shaft angle vs. time is controlled to follow a prescribed trajectory with two phases: a slow stance phase and a fast swing phase. The trajectories of two trials, (ω, ϕ) = (16 rad/s, 0.633) and (16 rad/s, 0.600), showing good repeatability. (d) Identical tripod trajectories produce different motion for ϕ = 0.600 and ϕ = 0.633. (e) For given limb frequency (ω = 4, 8, 12, 16, 20, 24, and 30 rad/s) the robot speed is remarkably sensitive to ϕ. Red and blue circles show the corresponding states in (c) and (d).

Fig. 2. Average robot forward speed vs. limb frequency. (a) For a given volume fraction ϕ, $\overline{v}_x$ increases sub-linearly with ω to a maximal average speed $\overline{v}_x^*$ at a critical limb frequency ω_c above which the robot fails ($\overline{v}_x < 2$ cm/s). The solid lines and symbols are for $\phi = 0.580$, 0.590, 0.600, 0.611, 0.616, 0.622, and 0.633. The dashed lines are fits from a model discussed in the text. (b)(c) The dependence of ω_c and $\overline{v}_x^*$ on ϕ shows transitions at $\phi \approx 0.6$ (dashed lines).

Fig. 3. Schematic of a single leg of the robot during a step in granular media. After a limb reaches the maximum penetration depth d_{max}, it rotates about its center and propels the robot forward a step length s. The solid shape denotes the initial stage of the rotational motion and the dashed shape indicates when the limb begins to withdraw from the material (final walking stage). (b) Step length as a function of ω derived from $\overline{v} = s\omega/2\pi$ reveals the condition for the onset of swimming, when $s < s_c = 7$ cm.

.

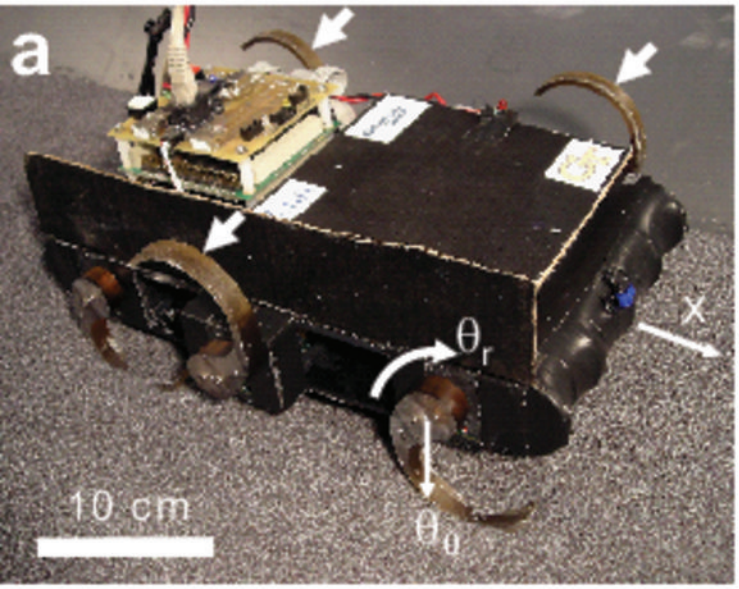
a
10 cm
θ_r
θ_0
x

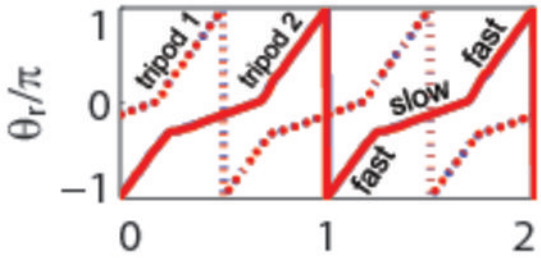
c
θ_r/π
tripod 1
tripod 2
slow
fast
fast
1
0
−1
0
1
2

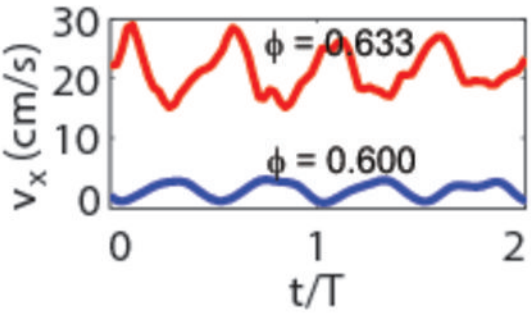
d
v_x (cm/s)
ϕ = 0.633
ϕ = 0.600
30
20
10
0
0
1
2
t/T

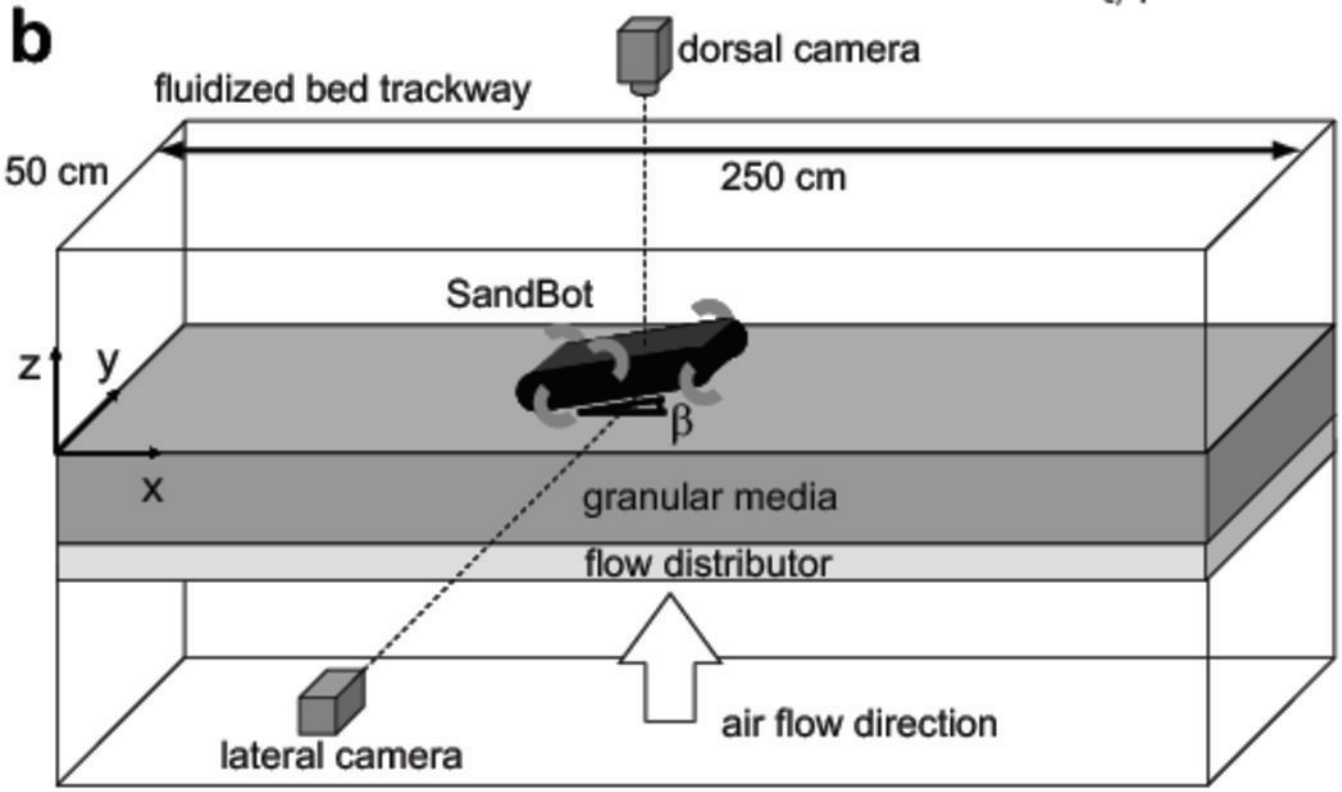
b
dorsal camera
fluidized bed trackway
50 cm
250 cm
SandBot
z
y
x
β
granular media
flow distributor
air flow direction
lateral camera

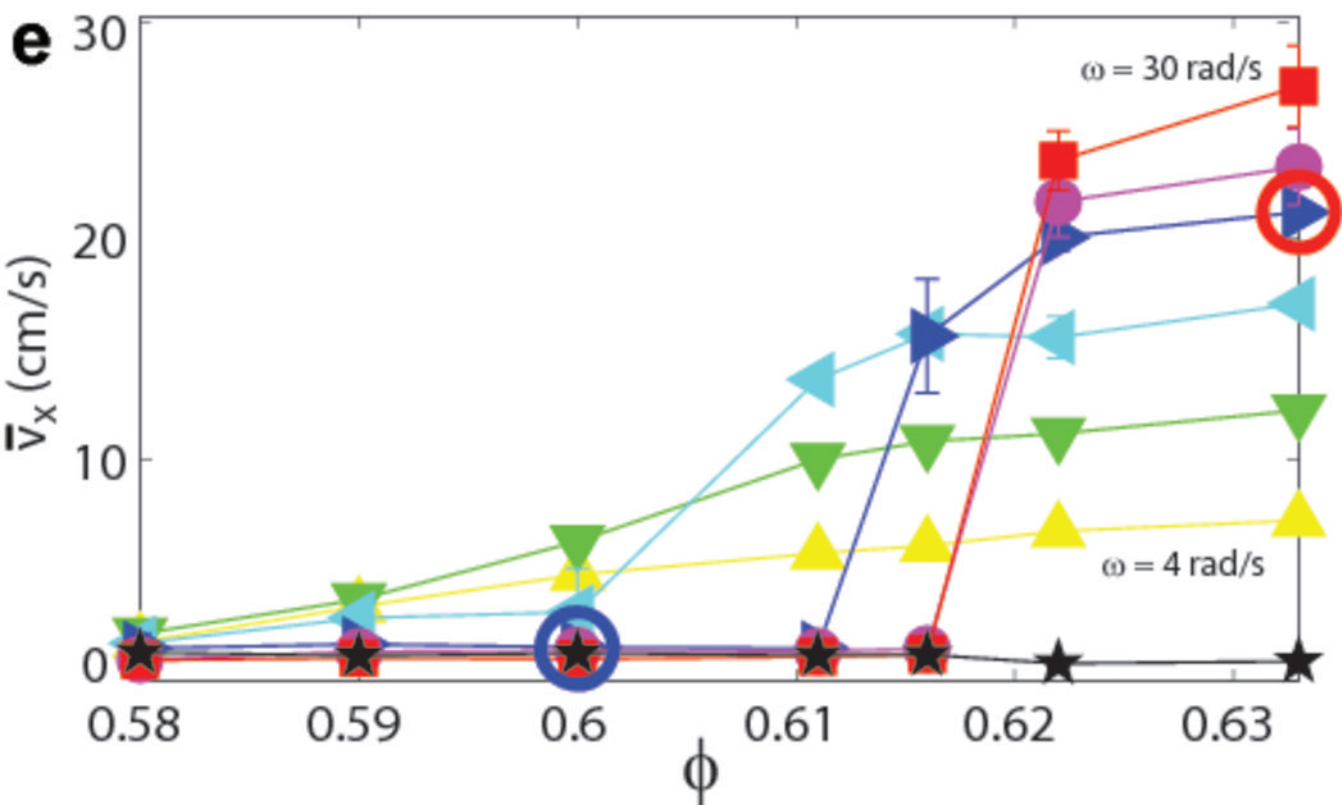
e
$\bar{v}_x$ (cm/s)
30
20
10
0
ω = 30 rad/s
ω = 4 rad/s
0.58
0.59
0.6
0.61
0.62
0.63
ϕ

a

$(\omega_c, \bar{v}_x^*)$

$\phi = 0.633$

walking

$\phi = 0.616$

swimming

$\phi = 0.580$

$\bar{v}_x$ (cm/s)

30
20
10
0

0
10
20
30

w (rad/s)

b

ω_c (rad/s)

30
20
10

0.58
0.6
0.62

ϕ

c

$\bar{v}_x^*$ (cm/s)

30
20
10
0

0.58
0.6
0.62

ϕ

a

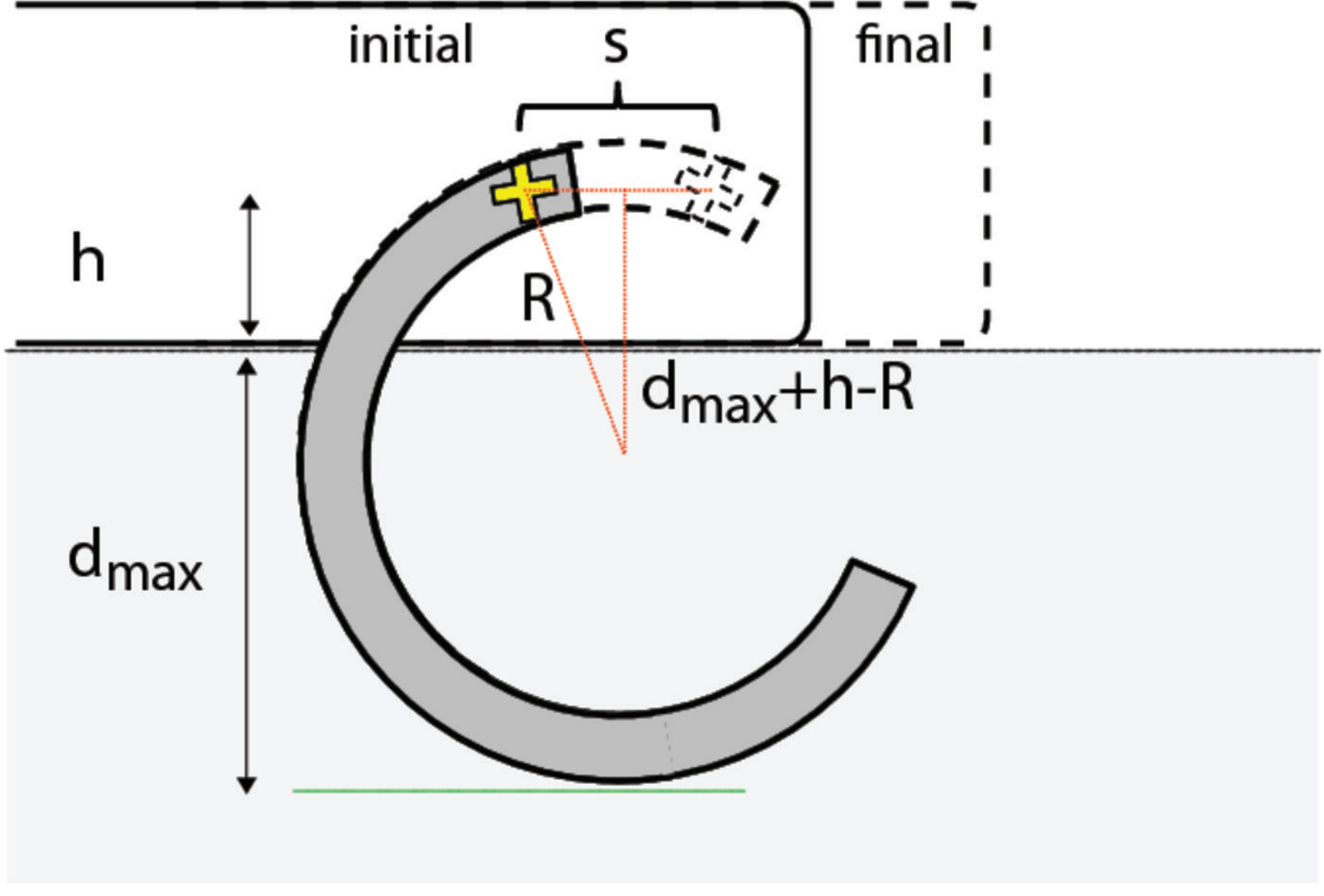
initial
s
final
h
R
d_{max}+h-R
d_{max}

b

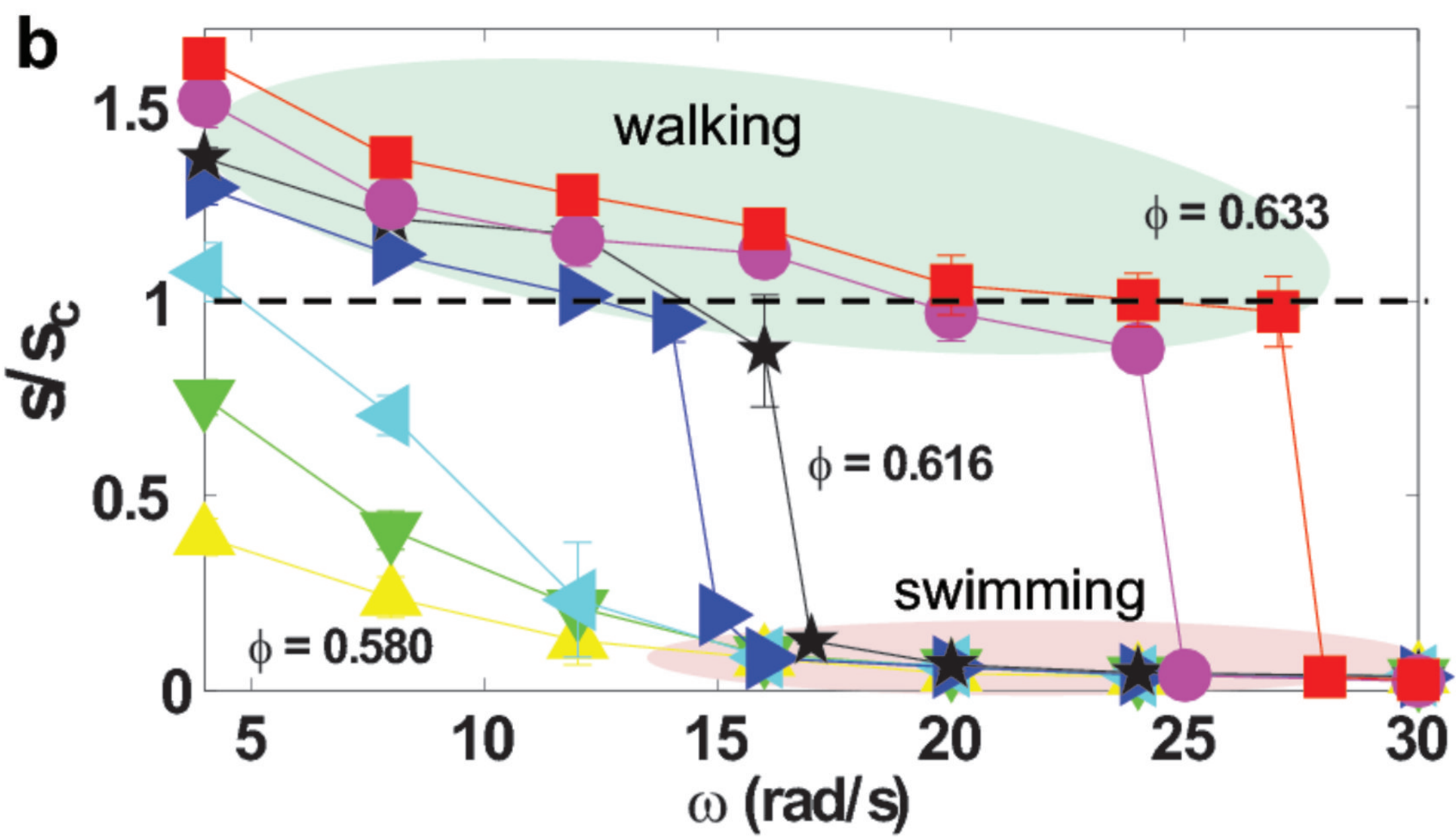
walking
swimming
ϕ = 0.633
ϕ = 0.616
ϕ = 0.580
s/s$_c$
ω (rad/s)
1.5
1
0.5
0
5
10
15
20
25
30